



Cite this: *Phys. Chem. Chem. Phys.*,
2014, 16, 26221

Rotationally resolved water dimer spectra in atmospheric air and pure water vapour in the 188–258 GHz range†

E. A. Serov, M. A. Koshelev, T. A. Odintsova, V. V. Parshin and M. Yu. Tretyakov*

New experimental results regarding “warm” water dimer spectra under equilibrium conditions are presented. An almost equidistant series of six peaks corresponding to the merged individual lines of the bound dimer with consecutive rotational quantum numbers is studied in the 188–258 GHz frequency range in water vapour over a broad range of pressures and temperatures relevant to the Earth’s atmosphere. The series is a continuation of the sequence detected earlier at lower frequencies at room temperature. The signal-to-noise ratio of the observed spectra allowed investigating their evolution, when water vapour was diluted by atmospheric air with partial pressure from 0 up to 540 Torr. Analysis of the obtained spectra permitted determining the dimerization constant as well as the hydrogen bond dissociation energy and the dimer spectral parameters, including the average coefficient of collisional broadening of individual lines by water vapour and air. The manifestation of metastable states of the dimer in the observed spectra is assessed. The contribution of three possible pair states of water molecules to the second virial coefficient is evaluated over the broad range of temperatures. The work supports the significant role of the water dimer in atmospheric absorption and related processes.

Received 22nd July 2014,
Accepted 6th October 2014

DOI: 10.1039/c4cp03252g

www.rsc.org/pccp

1. Introduction

The water vapour is the most important atmospheric absorber of the incoming Sun radiation and the Earth’s heat emission, thus strongly influencing the weather and climate.^{1,2} The climate models and prognoses based on them are very sensitive to the physical properties of water vapour and especially to the quantitative characteristics of its absorption spectrum. Along with the dominating absorption by water vapour resonance lines, which are concentrated in rovibrational bands, the water vapour continuum is also known as an essential contributor to the integrated absorption.³ The correct accounting of the continuum is important for the development of accurate climate models as well as for refining radiation propagation models used for retrieving the atmospheric parameters from the information coming from ground based, airborne and satellite remote sensing stations.

The old question about the contribution of different physical mechanisms leading to continuum absorption in the atmosphere has not been solved yet. In particular, the role of water dimers has been discussed for several decades.^{3–5} The evidence

of the dimer absorption within the IR water vapour absorption bands was demonstrated recently.⁶ However, its contribution to the continuum between the bands in the windows of relative atmospheric transparency remains uncertain.⁷ The main reason of the uncertainty is a very small value of the continuum absorption in the windows under atmospheric conditions. Another reason for the difficulties is insufficient information about the dimer spectral characteristics under ambient conditions. Until recently, direct observation of resolved rotational lines of the dimer was only possible in cold molecular beams, at temperatures of about several Kelvin.^{8–11} These spectra allowed determining the equilibrium configuration of the dimer and understanding its complicated intramolecular dynamics. Moreover, these spectra has strongly supported the development of *ab initio* calculations of the dimer potential energy surface, which allowed, in particular, assessing the dimer equilibrium constant under atmospheric conditions.^{12,13} However, all these studies could not give direct experimental evidence of the dimers’ presence in the atmosphere and determine their concentration.

Our recent work¹⁴ was the key step in determining the true role of dimers in atmospheric processes.¹⁵ The spectrum, unambiguously interpretable as belonging to the bound water dimer, was registered in pure water vapour at room temperature in the millimeter wavelength range. The observed spectrum clearly revealed the sequence of four peaks, each of which corresponds to the merged group of lines of the rotational

Institute of Applied Physics of the Russian Academy of Sciences, 46 Ul’yanov str., 603950, Nizhny Novgorod, Russian Federation. E-mail: trt@appl.sci-nnov.ru

† Electronic supplementary information (ESI) available. See DOI: 10.1039/c4cp03252g

spectrum of the dimer. Analysis of the spectrum and its comparison with the results of *ab initio* calculations¹⁶ led to the conclusion that the largest fraction of the millimeter-wave continuum absorption in water vapour at room temperature is due to the dimers.

The work¹⁴ demonstrated the possibility of dimer spectrum observation in warm water vapour. The next expected steps in this direction should be getting quantitative characteristics of dimer spectra, obtaining temperature dependence of these characteristics and, the most important for applications, direct observation of the dimer spectra in air. Analysis of the simplified model¹⁷ of the “warm dimer” spectrum developed on the basis of *ab initio* calculations and the first experimental data showed that the 1.2 mm transparency microwindow of the atmosphere located between intense water monomer lines centred near the frequencies of 183 and 325 GHz is most favourable for the observation of dimer spectra under ambient conditions.

All these steps were realized in the present work. The paper presents experimental recordings of the dimer spectra under various conditions, quantitative analysis of the spectra and the conclusions based on the findings of this analysis.

The details of the experimental method are presented in Section 2. Section 3 deals with the contribution of monomer lines. The results of analysing the spectra recorded in pure water vapour and in its mixture with the atmospheric air are given in Sections 4 and 5, respectively. The most important results are summarized in the Conclusion.

2. Experimental details

The method of measurements and the principle of operation of the resonator spectrometer used in this study are described in detail in the previous studies.^{18,19} The spectrometer measures the absorption coefficient of a gas mixture over a wide range of temperatures and pressures relevant to the Earth’s atmosphere. The module of two quasi-optical Fabry–Perot resonators was placed in a stainless steel chamber, thermally isolated from the environment, having a volume of about 200 litres. The total pressure of the gas mixture inside the chamber was controlled by the MKS Baratron pressure gauge (Type 626 of the 0.1–1000 Torr range) with a declared accuracy of 0.15%. The temperature of the gas and resonator mirrors was monitored using eight thermal resistors with an accuracy of ± 0.5 °C. To reduce the temperature gradients inside the chamber the resonators were placed inside a copper casing with a wall thickness of 5 mm. The gas temperature inside the chamber was controlled by the Julabo FP50 thermostat, which maintained the temperature of the refrigerant in the internal circuit within ± 0.01 °C near the preset value ranging from –50 to +200 °C. The refrigerant was circulated through the copper tube attached to the copper casing. The equilibrium temperature gradients inside the chamber in the studied range of temperatures did not exceed 2 °C.

The gas filling and pumping system contained the turbo and oil-free pump station (Pfeiffer, HiCube-80), as well as the

high-performance oil-free spiral pump for wet gases (Anest Iwata, DVSL-500C).

The OB-24 backward wave oscillator tube served as a source of continuous coherent radiation. The tube provided the power needed for the spectrometer operation in the frequency range from 188 up to 258 GHz. A 4 µm thick Teflon film was used for coupling the resonator with the radiation source and with the resonator response detector. The hydrophobic nature of this film²⁰ is important for reducing the influence of water adsorption on the result of water vapour absorption measurements.¹⁸

The principle of gas absorption measurement is based on determining the Fabry–Perot resonator Q-factor. The Q-factor depends on the total energy loss of an electromagnetic wave in the resonator, including the loss in the gas. In the approximation of small optical thickness, which was well satisfied under the conditions of the experiments, the absorption coefficient of the gas sample can be determined from measurements of the loss, when the resonator is filled with the sample gas and when it is filled with a non-absorbing gas (baseline or apparatus function),²¹ using the formula

$$\alpha = \frac{2\pi}{c}(\Delta f - \Delta f_0) \quad (1)$$

where α is the absorption coefficient, c is the speed of light in gas, Δf and Δf_0 are, respectively, the widths of the resonance curve of the resonator filled with the studied gas and with the non-absorbing gas.

In the case of wet gases, this principle of measurements can cause an additional systematic error related to adsorption of water molecules onto the mirrors and coupling films of the spectrometer, which leads to an uncontrolled change in its baseline.¹⁸ The cavity length variation method employed in our previous studies²² allows minimizing the aforementioned error by using two Fabry–Perot resonators. However, the “back side” of the method is reduction of the spectrometer sensitivity by about a factor of two. Such a reduction was considered to be inadmissible in this study because the contrast of water dimer peaks approaches the spectrometer sensitivity limit. To estimate the influence of the adsorption of water molecules in the present configuration of the spectrometer we performed a trial in which the absorption of water vapour at room temperature was measured using the length variation method with two resonators.¹⁸ The spectrum obtained using only one resonator coincided with the “true” spectrum obtained by the length variation method within the statistical uncertainty of the data. This result supported our decision to use only one resonator with a fixed length of about 70 cm in this work. The same resonator was used in the previous work.¹⁴

The resonant curve width was measured at the frequencies of the eigen modes. The spacing between the modes was approximately 200 MHz. About 310 eigen modes were selected within the 188–258 GHz range.

Before each series of measurements, the chamber was evacuated. The spectrometer baseline recording was obtained using the chamber filled with argon. The argon pressure was adjusted to the value, when its refractive index coincided with

the refractive index of the investigated sample. In this case, the eigen mode frequencies remained unchanged when argon was replaced by the sample gas. This method permits minimizing the possible systematic error caused by the resonator Q-factor modulation by unavoidable standing waves in the quasi-optical path of the spectrometer. After baseline recording, the chamber was evacuated and water vapour evaporating from the liquid phase was let into the chamber (the sample of double-distilled water was preliminarily cleaned from the dissolved atmospheric gases by freezing). Evaporation was carried on until the pressure in the chamber reached about 60% of the saturated water vapour pressure at a given temperature (~ 13 Torr at room temperature). In about 20 minutes after the pressure inside the chamber has stabilized, the resonance curve width measurements were started.

A total of 13 pure water vapour spectral recordings at temperatures ranging from 280 up to 322 K and vapour pressure from 3.7 to 34.2 Torr were made. The experimental absorption spectra can be found in the ESI.[†] Furthermore, a series of experiments with water vapour diluted with air were carried out. The details of the latter experiments are described in Section 4.

3. Experimental data processing: the monomer contribution

The total measured absorption was considered to have two major constituents, namely, regular resonant lines and continuum. Therefore, the continuum including the water dimer absorption spectrum can be found by subtracting the monomer spectrum from the total one:

$$\alpha_{\text{cont}} = \alpha_{\text{total}} - \alpha_{\text{lines}}, \quad (2)$$

where α_{cont} is the continuum absorption coefficient, α_{total} is the total absorption of the gas mixture derived from primary experimental data using eqn (1), α_{lines} is the contribution of the monomer lines to the absorption in the studied frequency range. The latter spectrum was calculated as a line by line sum of individual profiles using their spectroscopic parameters from the HITRAN 2012 database²³ and, if available, from experimental studies.^{24–31} Five most abundant water isotopologues (H^{16}OH , H^{17}OH , H^{18}OH , H^{16}OD , and D^{18}OH) in the ground vibrational state and H^{16}OH in the excited bending state were considered. All significant transitions with frequencies less than 1100 GHz were taken into account.

By analogy with our previous^{14,22} and many other studies and to allow the direct comparison with the results of these studies, the shape of the resonance lines was modelled by the function based on the Van Vleck–Weisskopf profile. The violation of the impact approximation at large detuning from the line centre was taken into account by “cutting” the wings of the profile beyond the cut-off frequency, ν_c , which approximately corresponds to the duration of intermolecular collision $\tau_c = 1/(2\pi\nu_c)$. The truncated line was then lowered to the zero level at the cut-off frequency, so that the final line shape function was

$$f_{\text{VWV}}^C(\nu) = \frac{\pi\nu^2}{\nu_0^2} \cdot (f_{\text{LC}}(\nu, \nu_0) + f_{\text{LC}}(\nu, -\nu_0)), \quad (3)$$

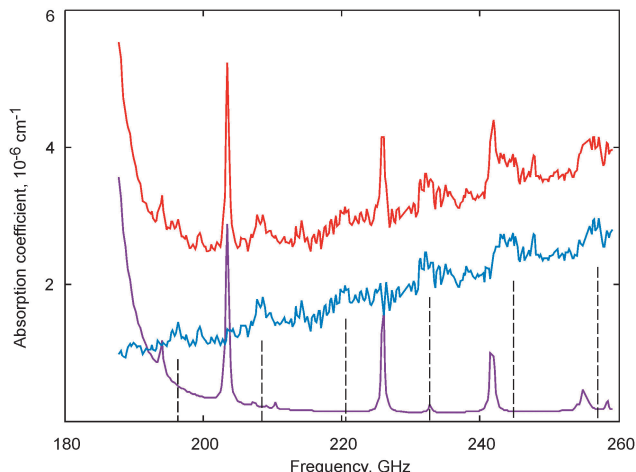


Fig. 1 Experimental recording of the absorption spectra of water vapour at 296 K and 12 Torr (upper trace – total absorption), the calculated spectrum of water monomer resonance lines (lower trace), and the derived (eqn (2)) continuum absorption (middle trace – this spectrum is shifted down by 10^{-6} cm^{-1} for figure clarity). The dashed vertical bars correspond to the positions of $J+1 \leftarrow J, K=0, E_1$ water dimer transitions calculated from the experimentally determined constants.⁹

$$f_{\text{LC}}(\nu, \pm \nu_0) = \begin{cases} \frac{\gamma}{(\nu \pm \nu_0)^2 + \gamma^2} - \frac{\gamma}{\nu_c^2 + \gamma^2}, & |\nu \pm \nu_0| < \nu_c \\ 0, & |\nu \pm \nu_0| \geq \nu_c \end{cases} \quad (4)$$

where ν_0 and γ are the central frequency and the half-width of the resonance line respectively. Note that this procedure leaves a small fraction of the resonance absorption in the continuum. For typical atmospheric conditions, the cut-off frequency is usually set to 25 cm^{-1} (750 GHz).³² The impact of the “cutting” on the quantitative characteristics of the observed continuum absorption will be assessed in the next section.

In the studied frequency range the most prominent contribution to the total absorption comes from the upper wing of the strong 183 GHz water line (Fig. 1). Relatively weak lines centered near 194 GHz, 203.5 GHz, 226 GHz, 242 GHz and 255 GHz are also quite noticeable.

Fig. 1 shows an example of experimental recording of the water vapour spectrum at 298 K and 12 Torr together with the calculated contribution of the monomer lines and the continuum absorption spectrum obtained in accordance with eqn (2). The continuation of the previously observed sequence of dimer peaks¹⁴ is clearly seen in the figure. The positions of the peaks are in good agreement with the $J+1 \leftarrow J, K=0, E_1$ water dimer rotational transition frequencies.⁹

4. Experimental data processing: contribution of bound dimers

We used the results of the most accurate to date *ab initio* calculations of the bound water dimer spectrum¹⁶ for determining the dimer contribution to the observed continuum. Direct quantitative comparison is impossible due to the complexity of the spectrum

and some significant differences of the *ab initio* spectra from the real data.^{14,17} The problem was solved by developing an approximate empirical model of the dimer spectrum reported earlier.¹⁷ The dimer spectrum was approximated by the sum of Lorentzians and the pedestal with the quadratic frequency dependence:

$$\alpha(\nu, T, p) = \left[\frac{A_0}{\pi} \sum_J \frac{\gamma_J I_J}{(\nu - \delta_J)^2 + \gamma_J^2} + A_2 \cdot \nu^2 \left(\frac{T_0}{T} \right)^{m2} \right] \cdot \left(\frac{T_0}{T} \right)^{m1} \cdot p^2, \quad (5)$$

$$\delta_J = 11.239 \cdot (J+1) + 8.68 \times 10^{-9} \cdot (J+1)^5 \quad (6)$$

$$I_J = J^4 \exp(-\lambda J) \quad (7)$$

$$\gamma_J = \eta J - \beta \cdot J^3 + A_1, \quad (8)$$

where α is the absorption coefficient in cm^{-1} , p is the pressure of water vapour in Torr, T is temperature in Kelvin, $T_0 = 296 \text{ K}$, A_0 , A_1 , A_2 , λ , η , β , $m1$ and $m2$ are constants, δ_J and γ_J are the central frequencies and half-widths of the dimer peaks in GHz, I_J is the relative integrated intensity of the peaks, and J is the number of peaks corresponding to the quantum number of the rotational transition $J+1 \leftarrow J$. Summation in eqn (5) is up to $J = 35$, which ensures a satisfactory approximation of the *ab initio* spectra by the model in the 60–350 GHz range. It should be noted that the model incorporates the temperature dependent water dimer equilibrium constant from ref. 33.

In this work, the model was optimized for the 188–258 GHz range. The constants of the model were varied to attain the best coincidence with the *ab initio* spectra in the particular frequency range, where dimer peaks with the J numbers similar to the ones observed in the experiment are located (6 peaks with J ranging from 15 up to 20). This range differs slightly from the experimental one because of imperfection of the peak positions in the *ab initio* spectrum.¹⁷ Such referencing to the peak numbers is based on the assumption that the *ab initio* calculation gives a correct dependence of integrated intensity of lines *versus* J , although the lines are predicted at slightly different frequencies.

The best-fit constant values derived from such optimization of the model to the *ab initio* spectra are:

$$A_0 = 0.663 \times 10^{-12} \text{ cm}^{-1} \text{ GHz Torr}^{-2}, \lambda = 0.0872, \eta = 0.108 \text{ GHz}, \\ \beta = 4.43 \times 10^{-5} \text{ GHz}, A_1 = (-0.91 + 0.037 \cdot p) \text{ GHz}, A_2 = 0.281 \times 10^{-12} \text{ cm}^{-1} \text{ GHz}^{-2} \text{ Torr}^{-2}, m1 = 12.3, m2 = -2.3. \quad (9)$$

The comparison of the optimized model (5) and the *ab initio* spectrum of bound dimers in pure water vapour at 296 K and 13 Torr in the 170–240 GHz range is shown in Fig. 2. Note that outside this range the optimized model is diverging from the *ab initio* spectra.

It was shown¹⁷ that the use of model (5) for experimental spectrum processing requires: (i) replacing the peak frequencies with values known from the experiment; (ii) adding two variable parameters: one corresponding to the additional width (the same for all peaks) and the other being a multiplier for the

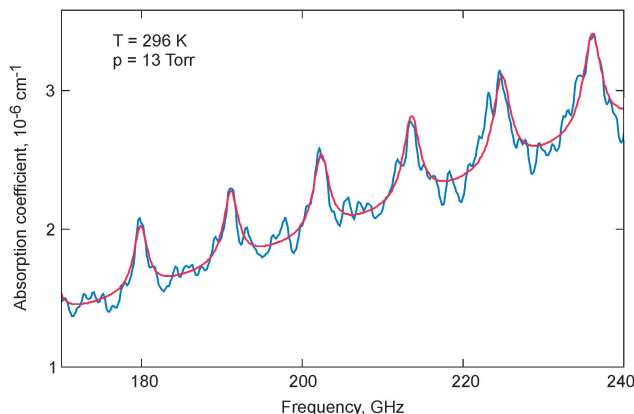


Fig. 2 The *ab initio* spectrum of bound water dimers as shown by a broken blue line (calculations reported by Scribano and Leforestier¹⁶ were used; the individual dimer line width was calculated on the basis of the 30 MHz Torr^{-1} pressure broadening coefficient³⁴). Model function (5) with constants from eqn (9) is shown by a smooth red line.

amplitude of the spectrum; and (iii) including an additional term smoothly depending on the frequency, which is responsible for the mechanisms of continuum absorption other than the bound dimer one.

The dependence of the frequency of the dimer peak on its number J was determined using both sets of the experimental data obtained in cold molecular beams (high accuracy measurements of the $J+1 \leftarrow J, K=0, E_1$ transition frequencies up to 110 GHz are available⁹) and our experimental spectra. It should be noted that in the spectra of the “warm” dimer, the coincidence of the central frequencies of the observed peaks (that are a superposition of a very large number of dimer lines corresponding to different ro-vibrational states) with frequencies of the $J+1 \leftarrow J, K=0, E_1$ rotational transition series of the ground vibrational state calculated from the cold beam measurements is not a general rule. However, the result of our previous study¹⁴ evidences that the deviation of frequencies is rather small for small J numbers. The following formula was obtained by fitting its coefficients to the aforementioned data:

$$\nu_J = 12.326 \cdot (J+1) - 3 \times 10^{-4} \cdot (J+1)^3, \quad (10)$$

where ν_J is the central frequency of the peak in GHz.

Finally, we came to the following model for processing of experimental spectra:

$$M_1(\nu, T, p) = \left(C_0 \left[\frac{A_0}{\pi} \sum_J \frac{\gamma_J J^4 \exp(-\lambda J)}{(\nu - \nu_J)^2 + \gamma_J^2} + A_2 \cdot \nu^2 \left(\frac{T_0}{T} \right)^{m2} \right] \right. \\ \left. \times \left(\frac{T_0}{T} \right)^{m1} + C_2 \cdot 10^{-12} \cdot \nu^{2.1} \right) \cdot p^2, \quad (11)$$

where the parameters A_0 , λ , A_2 , $m1$, and $m2$ are taken from (9), ν_J is taken from (10), $\gamma_J = 0.108J - 4.43 \times 10^{-5}J^3 - 0.91 + C_1$ is the width of the peak in GHz, and C_0 , C_1 and C_2 are adjustable parameters. The parameter C_0 corresponds to the amount of bound dimers under experimental conditions normalized by

their amount calculated *ab initio* in ref. 33. The parameter C_2 characterizes the additional absorption caused by the other mechanisms responsible for the continuum. Both C_0 and C_2 depend on temperature. The parameter C_1 defines the width of the experimentally observed dimer peaks. In the first approximation it should have linear dependence on the water vapour pressure. Its dependence on temperature was neglected. The term corresponding to additional non-resonance absorption in model (11) is proportional to ν^{2-1} because such dependence was found to be in better agreement with the experimental data than the usual quadratic one.

The M_1 model was used for processing of 13 experimental spectra of pure water vapour (10 of them were registered at temperatures near 296 K). As an example, Fig. 3 shows the result of the model fitting to the spectrum obtained at 311.1 K and 27.2 Torr. In this spectrum, the signal-to-noise ratio of the dimer peaks ($S/N \sim 24$) is better than that of the spectra obtained at room temperature ($S/N \sim 7$). The value of the continuum absorption determined on the basis of the experimental data from our earlier work²² is also shown in the figure for comparison. The averaged difference between this continuum, which was derived from absorption measurements in wet nitrogen at atmospheric pressure, and the spectrum of pure water vapour constitutes 5%, which can be considered as good agreement.

Fig. 4 shows the dependence of the parameter C_1 on the pressure of water vapour and its linear approximation: $C_1 = 0.18(7) + 0.013(3)p$. It follows from the plot that the average coefficient of dimer line broadening by water vapour pressure can be estimated to be 13(3) MHz Torr⁻¹.

The values of C_0 and C_2 parameters obtained from the spectra recorded at different temperatures are presented in Fig. 5. Ten values corresponding to the near-room-temperature data were averaged and shown as one point in this figure. The obtained data did not reveal any evident dependence of C_0 on temperature. The average value of this parameter is 0.67(6).

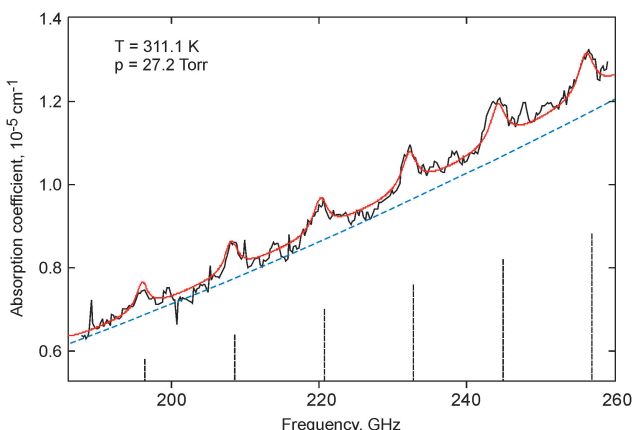


Fig. 3 Continuum absorption in water vapour. Experimental recording is shown by the broken black line. The smooth red line shows model (11) optimized to the experimental spectrum. The dashed blue line shows the empirical model of continuum absorption.²² The positions of $J + 1 \leftarrow J$, $K = 0$, E_1 water dimer transitions are shown by dashed vertical bars.

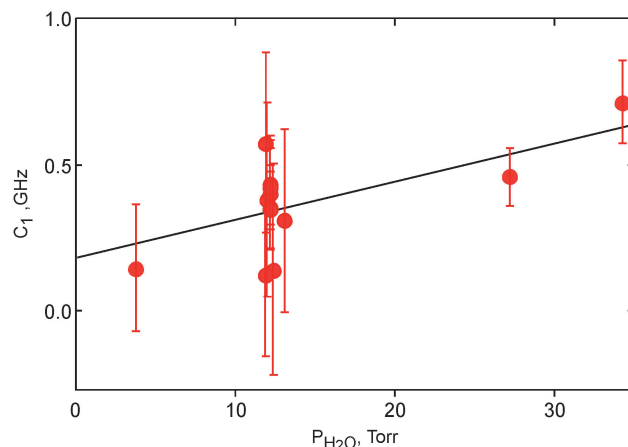


Fig. 4 Pressure broadening of the dimer peaks. Measured values of the model parameter C_1 defining the width of the dimer peaks are plotted versus water vapour pressure (circles). The solid line is the result of linear approximation of these points. The vertical bars correspond to one standard deviation of experimental data.

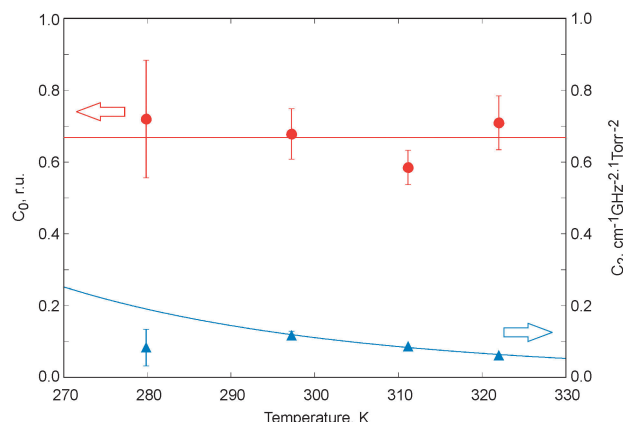


Fig. 5 Temperature dependence of the parameters C_0 (red circles, relative units) and C_2 (blue triangles, $\text{cm}^{-1}\text{GHz}^{-2.1}\text{Torr}^{-2}$). The specified uncertainties of the points correspond to one standard deviation. Solid lines approximating the points are explained in the text.

This means that: (i) the temperature dependence of the dimerization constant³³ of the bound dimer implicitly used in model (11) agrees with the experimental data within their uncertainties in the studied range of conditions; and (ii) the magnitude of this constant is on the average 67(6)% of the calculated value.³³

Let us now consider the last term in model (11) characterized by the parameter C_2 and the corresponding absorption determined from the experimental data. To study the origin of this additional absorption it is necessary to recall all possible mechanisms responsible for the continuum in water vapour.

The “bimolecular absorption” was suggested⁶ as a physical mechanism fully explaining the origin of the water continuum. This approach is based on partitioning of the molecular pair states into true bound (stable) dimers, quasi-bound (metastable) dimers and free pairs.^{35–37} The continuum associated with dimer states is, in fact, a conventional resonance absorption of radiation

by a double molecule. The lines of this molecule can be additionally broadened due to the short lifetime of the metastable state. The absorption resulting from free pairs is caused by the additional transient dipole moment induced in a single molecule during single-approach collisions of two unbound monomers. The continuum related to the above-mentioned problem of far wings of monomer lines can also be interpreted in terms of bimolecular absorption as the result of inelastic collisional interaction of two unbound monomers. However, it is worth mentioning that the shape of the resonance line is formed by cumulative contribution of all single molecules flying from one collision to another one. The contributing single molecule can form either a free pair state or a metastable dimer with the next collision's partner.

It follows from the previous estimates^{37–39} that the contribution of free pairs, as well as the contribution of far wings of the monomer lines to the continuum absorption, is negligible under the conditions of our experiments. Absorption by bound water dimers is taken into account by the first summand in parenthesis of model (11). Therefore, the second summand is apparently responsible for the spectrum of metastable water dimers.

Regarding the temperature dependence of the parameter C_2 it should be noted that the value obtained at the lowest temperature significantly diverges from the expected pattern. The most likely reason of this divergence is the low signal-to-noise ratio (the water vapour pressure in this experiment was lower by a factor of 3.5 in comparison with the room temperature experiments, whereas the continuum is proportional to the squared pressure) and the lack of repeated recordings. Neglecting this point, the temperature dependence of the remaining data can be approximated by a conventional power function: $C_2 = 0.12 \cdot (296/T)^{7.8} \text{ cm}^{-1} (\text{GHz}^{2.1} \text{ Torr}^2)^{-1}$. The exponent of this function is smaller than the corresponding value of 10.67 calculated for bound dimers¹⁶ and is close to 8.24(21) resulting from our study of the continuum in the $\text{H}_2\text{O} + \text{N}_2$ mixture at atmospheric pressure in the 107–143 GHz frequency range.²² This relationship of the exponents is in qualitative agreement with the assumption, which is based on the analysis of our experimental data, that true bound and quasi bound dimers have comparable contributions to the total observed self-continuum under atmospheric conditions. Therefore, the “slope” of the temperature curve of this total absorption should have some intermediate value.

To verify the temperature dependence of the non-resonance absorption it is necessary to increase the sensitivity of the spectrometer and to carry out additional research. In this respect low-temperature measurements are the most interesting for atmospheric applications.

It was mentioned earlier that the “cropped” Van Vleck–Weisskopf profile with the 750 GHz cut-off frequency was used for the monomer spectral modelling. The derived continuum is systematically smaller, if the “non-cropped” profile is employed. We found that in this case fitting model (11) to the experimental data gives practically the same values of the parameters C_0 and C_1 , but the C_2 parameter is smaller by 5–6%. However, this small systematic deviation is comparable with the uncertainty

of the parameter value resulting from the fitting. Therefore, the trial confirms the insignificance of the far wing contribution to the observed continuum in the studied frequency range; moreover, it allows concluding that the far wing uncertainty does not affect significantly the quantitative characteristics of the bound dimers obtained from experimental spectra.

Another important aspect should be mentioned before continuing the data analysis.

Model (5) is not the only model that may be used for approximating the *ab initio* spectrum of the water dimer. The drawback of this model is potential correlation between the width of Lorentzians (C_1) and the amplitude of additional non-resonance absorption (C_2). To assess the influence of this correlation an additional data processing using Gaussian peaks in model (5) instead of the Lorentzians was performed. The correlation of parameters in such a model must be significantly smaller because of a sharp decay of the Gaussian function wings.

The corresponding model was developed and complete processing of experimental data was undertaken repeating all the steps described above.

Fig. 6 shows the result of approximation of the experimental spectrum by both models. The divergence between the two models is barely visible. The standard deviations of experimental points from the models are almost identical and constitute 9.65×10^{-8} and $9.77 \times 10^{-8} \text{ cm}^{-1}$ for the “Lorentzian” and “Gaussian” models, respectively. For the “Gaussian” model, C_0 and C_2 parameters and the slope of the linear dependence of the C_1 parameter on the pressure coincide with the corresponding parameters of the “Lorentzian” model within statistical uncertainty (Table 1). This coincidence means that the correlation of the peak amplitude and additional non-resonance absorption is insignificant. Two models are practically indistinguishable. Therefore, the obtained parameters are of equal value.

The convolution method

Analysis of sophisticated spectra containing many overlapping lines can be performed by using the convolution method elaborated by Pickett.⁴⁰ This method is based on the fact that the result of homogeneous spectrum broadening (*i.e.*, collisional broadening)

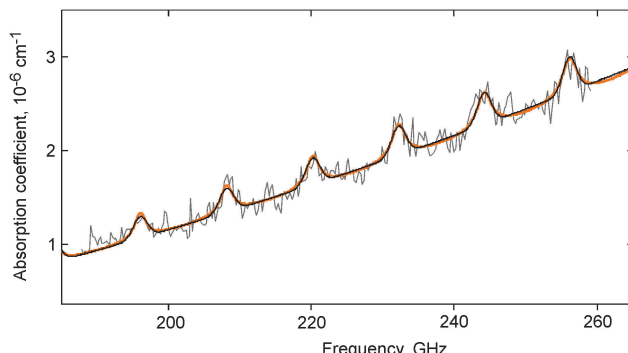


Fig. 6 Experimental spectrum of water vapour continuum absorption at 297.8 K and 12.1 Torr (broken grey line) and two models fitted to the experimental data. The smooth thin black line corresponds to the “Gaussian” model and the smooth thick orange line is for the “Lorentzian” one (see text).

Table 1 Parameters of the model functions with the Lorentzian and Gaussian peaks obtained by fitting to the experimental data

	$\langle C_0 \rangle$, rel. units	$\langle dC_1/dp \rangle$, MHz Torr $^{-1}$
“Lorentzian” model	0.67 (6)	13 (3)
“Gaussian” model	0.63 (6)	15 (4)
Averaged value	0.65	14

can be formally treated as an initial spectral profile modification by an integral operator. The operator is a convolution of the spectrum and the Lorentz profile. Let us denote the continuum absorption spectra observed at pressures p_1 and p_2 ($p_1 < p_2$) as $S_1(\nu, p_1)$ and $S_2(\nu, p_2)$, respectively. If the spectrum consists of the sum of blended lines of a bound dimer and a smooth base (corresponding to other absorption mechanisms), then the following relationship is valid:

$$S_2(\nu, p_2) = h_1 \cdot \int_{-\infty}^{\infty} S_1(\tilde{\nu}, p_1) \cdot \frac{\Delta\nu_c}{\pi} \cdot \frac{1}{(\nu - \tilde{\nu})^2 + \Delta\nu_c^2} d\tilde{\nu} + \Delta\Omega(\nu), \quad (12)$$

where $\Delta\nu_c = \gamma(p_2 - p_1)$, γ is the coefficient of pressure broadening of individual dimer lines by water vapour (which is assumed to be the same for all lines), h_1 is the factor corresponding to the variation of the integrated intensity of the bound dimer spectrum with pressure, and $\Delta\Omega(\nu)$ is the term related to the base variation. Analysis of the experimental data confirmed that the most appropriate frequency dependence of the base is $\nu^{2.1}$ (it corresponds to the minimum deviation of the model function from the experimental data). The requirement of infinite integration limits in eqn (12) is in formal contradiction to the spectra recorded within a finite frequency interval ($\nu_1 \leq \nu \leq \nu_2$). It was found that for modelling the water vapour spectra recorded at pressures ranging from 3.7 Torr to 34.2 Torr it suffices to extend the $S_1(\nu, p_1)$ spectrum to the regions $0.95\nu_1 \leq \nu < \nu_1$ and $\nu_2 < \nu \leq 1.05\nu_2$. The smoothed function $\langle S_1(\nu, p_1)/\nu^2 \rangle \cdot \nu^2$ was used as the spectrum extension, where averaging was over the 188–258 GHz range. Thus, eqn (12) takes the form:

$$S_2(\nu, p_2) = h_1 \cdot \int_{\nu_{\min}}^{\nu_{\max}} S_1(\tilde{\nu}, p_1) \cdot \frac{\gamma \cdot (p_2 - p_1)}{\pi} \times \frac{1}{(\nu - \tilde{\nu})^2 + \gamma^2 \cdot (p_2 - p_1)^2} d\tilde{\nu} + h_2 \cdot \nu^{2.1}, \quad (13)$$

where ν_{\min} and ν_{\max} are equal to 180 and 268 GHz, respectively.

In general, S_1 and S_2 spectra can be recorded at different temperatures. In this case eqn (12) can be correct, if γ is temperature independent. However, its dependence is usually close to $1/T$. The corresponding variation of the broadening coefficient at a temperature changing from 280 K to 322 K is about 15%, which is twice less than the uncertainty of the mean value of pressure broadening of the dimer spectrum (Table 1). This allows neglecting the temperature dependence of the broadening coefficient.

Determination of the mean pressure broadening coefficient of dimer lines by fitting model (13) to the experimental spectra is more appropriate than using model (11), because it does not

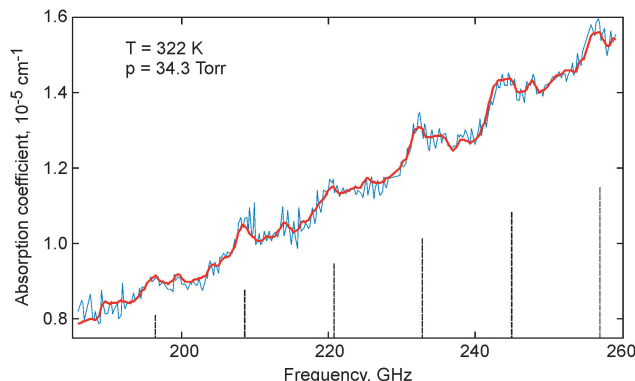


Fig. 7 Experimental recording of water vapour continuum absorption (thin blue line) and the “convolution model” (see the text) obtained from the spectrum recorded at 298.3 K and 12.1 Torr (thick red line). The positions of $J+1 \leftarrow J, K=0, E_1$ water dimer transitions are shown by dashed vertical bars.

assume a particular form of the dimer spectrum and results in the correct value even if the inhomogeneous component of the line width cannot be considered to be negligible in comparison with the homogeneous one. It is worth mentioning that this method gives quite a poor result if the spectra are recorded with large frequency steps and at close pressures.

Fig. 7 presents the experimental spectrum of water vapour continuum absorption recorded at 322 K and 34.3 Torr together with the other spectrum recorded at 298.3 K and 12.1 Torr and fitted to conditions of the first spectrum using eqn (13). The “convolution” is in perfect agreement with the real spectrum. This fact confirms that most of the large-scale spectrum features are not the experimental noise, but spectral peculiarities or “fingerprints” of the dimer.

All the pairs of available experimental spectra corresponding to different pressures were treated using the convolution method to determine the broadening coefficient value. The resulting dependence of $\Delta\nu_c$ on $(p_2 - p_1)$ is presented in Fig. 8. The difficulty of the convolution method in the case of a small pressure difference leads to a large uncertainty of $\Delta\nu_c$ determined from such pairs. The average broadening coefficient of the dimer lines was determined from these data by the median averaging method. This means that the points are averaged with the weight which is inversely proportional to the point difference from the mean value. Statistical uncertainty is large in this case (about 100%). Nevertheless, the broadening parameter value (13 MHz Torr $^{-1}$) coincides with the value obtained by using model (11). This value, therefore, can be used for modelling the dimer spectrum.

Water dimer spectrum shape

The most probable shape of the water dimer spectrum at 296 K and a water vapour pressure of 12 Torr can be obtained by averaging a series of spectra recorded under similar conditions. The minor difference in experimental pressures and temperatures can be taken into account using known values of the corresponding coefficients from the model (11). The result of

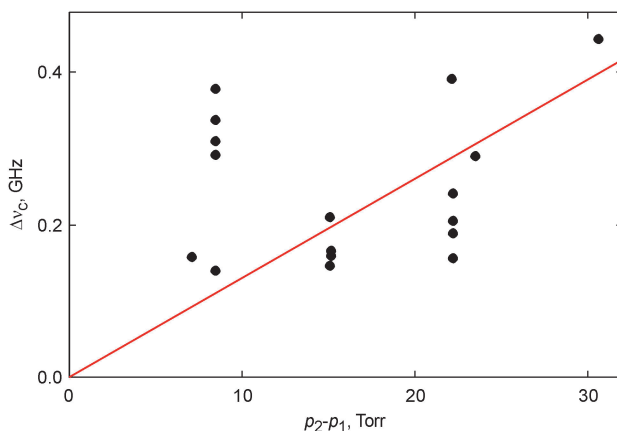


Fig. 8 Homogeneous line width from convolution method (13) versus experimental spectra pressure difference. The points are the result of experimental spectra processing, and the line corresponds to the dependence obtained by the median method (see the text).

such averaging of all 10 experimental spectral recordings at room temperature is shown in Fig. 9 together with the experimental points.

To check the quality of this averaged spectrum, we recalculated it using the convolution method for the conditions of the experimental spectrum (311.1 K, 27.2 Torr), which was obtained with the best signal-to-noise ratio during this experimental cycle. We used the formula similar to eqn (13). The broadening coefficient value was fixed at $\gamma = 13 \text{ MHz Torr}^{-1}$. To achieve the best fit the frequency dependence of the additional term was changed to $\nu^{2.6}$. It can be seen in Fig. 9 that these two spectra coincide up to the small spectral details. This coincidence allows claiming that all these details are not the experimental noise but peculiarities of the water dimer spectrum.

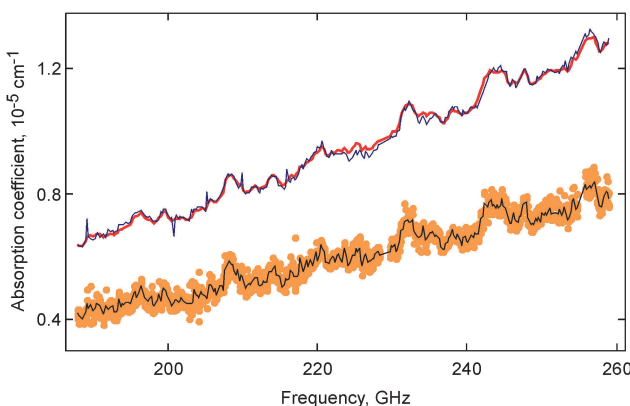


Fig. 9 Averaged spectrum of water dimer obtained from experimental recordings in pure water vapour at near room temperature and the result of its recalculation to the conditions of another experimental recording by the convolution method. The experimental data (recalculated to 296 K and 12 Torr) used for the averaging are shown by points, the averaged spectrum is shown by the solid black curve. All these room temperature data are shown with doubled amplitude for the convenience of their comparison with the experimental spectrum recording at 311.1 K and 27.2 Torr (blue line) and with recalculation of the averaged spectrum to these conditions (thick red line).

Dimer abundance in water vapour

It is known from statistical physics³³ that the dimerization constant K_D is directly related to the dimer dissociation energy D_0 :

$$K_{\text{Db}}(T) = \frac{p_{\text{Db}}}{p_M^2} = \frac{1}{kT} \frac{Q_{\text{VR}}^{\text{Db}} \exp(D_0/kT)}{\lambda_D^3} \left(\frac{Q_M^M}{\lambda_M^3} \right)^{-2}, \quad (14)$$

where K_{Db} is related to the bound states of the dimer only, k is the Boltzmann constant, the quantities related to the monomer and the dimer are indexed, respectively, by M and D (Db means bound dimer), Q_{VR} is the rovibrational partition function, and $\lambda = h/(2\pi mkT)$ is the de Broglie wavelength.

The value of C_0 in model (11) (Fig. 5) determined from the experimental spectra is, in fact, the ratio

$$C_0 = \frac{K_{\text{Db}}^{\text{exp}}}{K_{\text{Db}}^{\text{calc}}},$$

where the superscript "exp" corresponds to the experimentally determined value of the constant and "calc" is related to the theoretically calculated value.³³ It allows estimating the dimer dissociation energy D_0 from eqn (14) (assuming that the partition functions are calculated correctly) as:

$$D_0^{\text{exp}} = D_0^{\text{calc}} + kT \ln \frac{K_{\text{Db}}^{\text{exp}}}{K_{\text{Db}}^{\text{calc}}} \quad (15)$$

where $D_0^{\text{calc}} = 1234 \text{ cm}^{-1}$.³³ This value is included implicitly in our model of the dimer spectrum, eqn (11). The averaged value of D_0^{exp} obtained from eqn (15) is $1144(19) \text{ cm}^{-1}$. In spite of the complexity of the studied object and the quite modest set of experimental data this value of dissociation energy is in very reasonable agreement with 1108 cm^{-1} resulting from the recent *ab initio* calculations⁴¹ and with $1105(10) \text{ cm}^{-1}$ obtained experimentally by the velocity map imaging method.⁴²

The values of the bound dimer equilibrium constant $K_{\text{Db}}(T)$ obtained in this work are shown in Fig. 10 together with the dependence calculated by Scribano *et al.*³³ For the sake of comparison, the figure also presents the most reliable previous experimental data obtained through thermal conductivity measurements⁴³ and the $K_D(T)$ dependence calculated from the second virial coefficient using the approximate formula:

$$K_D(T) = \frac{b_0 - B(T)}{RT}, \quad (16)$$

where b_0 is the excluded volume, $B(T)$ is the second virial coefficient, and R is the gas constant.

As was mentioned above (Table 1), the K_{Db} value obtained from our data is about 35% smaller than the theoretical value.³³ A comparison with the experimental results⁴³ is not straightforward because of the temperature range difference; however, extrapolation of our data to the high temperature region (using the T -dependence of the constant³³) agrees with these results within their uncertainty limits. The experimental values⁴³ are systematically higher than the extrapolation curve. This can be explained by the metastable dimers, which contribute to thermal conductivity measurements but do not contribute to the periodic sequence of peaks in the spectrum.

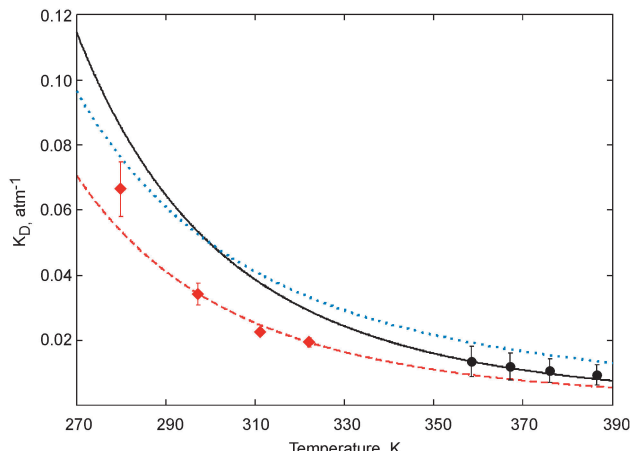


Fig. 10 Temperature dependence of the dimerization constant of water vapour. Experimental values obtained in this work for the bound dimers are shown by the red rhombuses (the vertical bars correspond to $\pm 1\sigma$ statistical uncertainty); calculations from the first principles³³ are shown by the solid black curve. The dashed red curve is the same dependence multiplied by 0.65 (Table 1); calculations from the second virial coefficient⁴⁴ are shown by the dotted blue curve. The black circles correspond to thermal conductivity measurement data⁴³ (in this case, error bars correspond to $\pm 0.5\sigma$).‡

Calculation of the constant from eqn (16) requires data on the second virial coefficient and on the excluded volume. The second virial coefficient was calculated on the basis of empirical data.⁴⁵ Accurate parameterization of these data in the range of 273–1273 K was performed in the earlier work.⁴⁴ The temperature dependence of the excluded volume was taken from the recent work,⁴⁶ in which $b_0(T)$ was calculated in the 200–600 K range as the classical excluded volume using the full dimensional potential energy surface of the dimer determined *ab initio*, which has been most accurate to date. Recall that eqn (16) gives the K_D value related to both bound and metastable dimers:

$$K_D = K_{Db} + K_{Dm},$$

where K_{Dm} is the dimerization constant related to metastable dimers.

It is known that the pair interaction of monomers is responsible for the second virial coefficient of the gas equation of state. It can be represented as the sum of three terms corresponding to the aforementioned pair states, namely free pairs, metastable dimers and bound dimers:^{35–37,47}

$$B(T) = B_{\text{free}} + B_{\text{metastable}} + B_{\text{bound}} = b_0 - K_{Dm}RT - K_{Db}RT \quad (17)$$

Therefore, available data, including K_{Db} obtained in this work, allow calculating relative contributions of bound dimers, metastable dimers and free pairs to the second virial coefficient in a quite broad range of temperatures. The absolute values of

‡ The authors of work⁴³ did not assess the possible uncertainty of the equilibrium constant. However, the uncertainty can be found using the analytical relationship of K_D with enthalpy (ΔH_2) and entropy (ΔS_2) of the dimer formation (eqn (11) from ref. 43). Their values were found, and their possible errors were analyzed in detail.⁴³

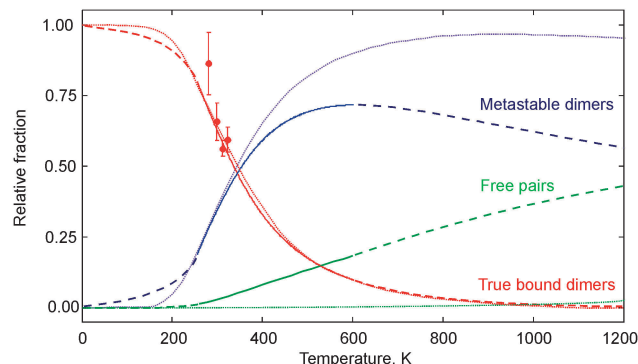


Fig. 11 The absolute value of the relative contributions of bound dimers (red curve), metastable dimers (blue curve) and free pairs (green curve) to the second virial coefficient of water vapour (solid and dashed curves) and to the total number of interacting pair states (dotted curves). The red circles present the results of calculations from our experimental data (see the text). The vertical bars correspond to the statistical uncertainty of one standard deviation. The dashed lines are extrapolations of the calculated dependence to low and high temperatures. The dotted lines correspond to the calculated dependence.³⁷

the aforementioned contributions *versus* temperature are shown in Fig. 11. The dashed lines in the figure correspond to a reasonable extrapolation of the dependences. In particular, the dominating amount of bound dimers at the low-temperature limit and the prevailing amount of free pairs at high temperatures were taken into account. Note that these extrapolations are not appropriate for quantitative evaluation studies.

It is interesting to compare this relative contribution of different molecular pairs to the second virial coefficient with the relative number of the corresponding pair states. For water vapour such calculations were performed by Vigasin³⁷ using truncated partition functions and a simplified interaction potential. The results of these calculations are also presented in Fig. 11 and demonstrate very good agreement with our data. Most pronounced is the coincidence of the curves related to bound dimers. The agreement confirms the main conclusions of Vigasin's work,³⁷ related to the role of water dimers in the Earth's atmosphere: "The fraction of bound states . . . is about 50%, the remainder being metastable states. There are practically no free states".

Additional nonresonant absorption

We now consider the non-resonant absorption related to the term with the C_2 parameter in model (11). This absorption constitutes about 50% of the total continuum absorption in pure water vapour at room temperature. As was mentioned above, metastable water dimers are the most probable origin of this absorption. Verification of this hypothesis requires knowledge of the metastable dimer spectrum. Rigorous calculations of the spectrum are not available yet. However, the simplified model of a metastable dimer as two monomers rotating almost freely near each other was proposed for estimations.^{6,48} The spectrum of such a pair of molecules should look like a doubled monomer spectrum homogeneously broadened by a short lifetime of metastable states. In accordance with the estimations

made by Ptashnik *et al.*,⁶ the individual linewidth in the spectrum of a metastable dimer should be within 7–20 cm⁻¹ (210–600 GHz), which corresponds to the lifetime of about 0.3–0.8 picoseconds. Following this model, we calculated the metastable dimer spectrum as the line by line sum of water monomer rotational transitions using the Van Vleck Weisskopf line shape. The frequencies and intensities of the transitions were taken from the HITRAN 2012 database.²³ The calculated spectrum in the 0–300 GHz range can be very well approximated by a power function of frequency $C \cdot \nu^y$. The value of the exponent y varies from 2.0 up to 2.4 depending on the chosen width of individual lines. It was mentioned above that the best fit of the experimental data was achieved with the additional absorption model function proportional to $\nu^{2.1}$. Such a frequency dependence of the spectrum was obtained when the line width in the model was set to 18 cm⁻¹ (the corresponding lifetime was 0.3 ps).

The final expression for the metastable dimer spectrum in units of the absorption coefficient (cm⁻¹) in the frequency range up to 300 GHz can be written as:

$$\alpha_{Dm1} = \frac{K_{Dm} \cdot p^2}{kT} I_0 \cdot \nu^{2.1} \quad (18)$$

where $I_0 = 2.38 \times 10^{-33}$ cm⁻¹ J atm per Torr² GHz^{2.1}. The value of K_{Dm} can be calculated from expression (17) using the K_{Db} values from experimental data. The spectrum was calculated and its temperature dependence was determined (Fig. 12). The calculated absorption proved to be less than the observed one by about an order of magnitude, demonstrating failure of the simplified model of the metastable dimer spectrum in this frequency range.

Another way to estimate the absorption caused by metastable dimers was proposed by Vigasin in ref. 37. It was suggested that

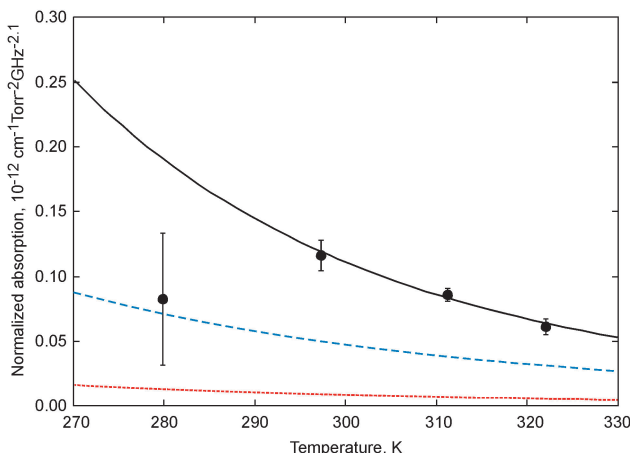


Fig. 12 Comparison of various models of the metastable dimer spectrum with experimental data on additional continuum absorption. The absorption is normalized to p^2 and $\nu^{2.1}$. The “doubled monomer” absorption model is shown by the red dotted curve. The “broadened bound dimer” absorption model is shown by the dashed blue curve. The circles correspond to experimentally determined C_2 values (model (11)). The solid black curve is the approximation of the experimental points by the function $0.12 \times 10^{-12} (296/T)^{7.8}$.

the spectrum “should be sufficiently close to the broadened spectra of the bound particles”. The corresponding absorption can be calculated on the basis of model (11), in which: (i) the parameter C_0 is multiplied by the metastable to stable dimers ratio (Fig. 11), (ii) the width of all peaks is increased by 15 GHz (with such broadening, the spectrum becomes blurred enough and a further increase of the peak widths does not change its smooth form), and (iii) the parameter C_2 is set to zero:

$$\begin{aligned} \alpha_{Dm2} &= C_0 \cdot \frac{K_{Dm}}{K_{Db}} \\ &\times \left[A_2 \cdot \nu^2 \left(\frac{T_0}{T} \right)^{m^2} + \frac{A_0}{\pi} \sum_J \frac{(\gamma_J + 15) \cdot J^4 \exp(-\lambda J)}{(\nu - \nu_J)^2 + (\gamma_J + 15)^2} \right] \\ &\times \left(\frac{T_0}{T} \right)^{m^1} \cdot p^2. \end{aligned} \quad (19)$$

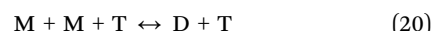
The temperature dependence of this absorption normalized to p^2 and $\nu^{2.1}$ is plotted in Fig. 12 by the dashed curve. It can be seen that the agreement with the experiment is not quite perfect but this model is much closer to the observed absorption than the first one.

Ab initio calculations of the metastable dimer spectrum could be very helpful to clarify its real contribution to the observed absorption and to continue the discussion about the origin of the continuum. However, to the best of our knowledge, such calculations are not feasible yet.

5. Experimental data processing: the dimer spectra in air

Some progress in understanding the real role of water dimer in atmospheric processes can be achieved by studying the changes in the dimer spectrum when air is gradually added to the pure water vapour.

The bound dimer (D) collisional formation from two monomers (M) is a reversible reaction including participation of some third body (T):



It is known that the equilibrium constant of the reaction should be independent of the features of the third body, because of the same interaction between the weakly bound pair of monomers, and the third body is responsible for both the stable dimer formation and the dimer destruction. The minor difference between the bound dimer formation in pure water vapour and in air should be related to the collisional formation of H₂O–O₂ and H₂O–N₂ heterodimers, which slightly reduces the number of monomers available for reaction (20).

The expected effect of adding air to water vapour is the collisional broadening of the dimer spectrum. However, the integrated intensity of the observed spectrum should remain unchanged if the concentration of dimers is unchanged.

This section presents the first results regarding the observation of the bound dimer spectrum in ambient air.

The gas mixture for the trial was prepared using laboratory air. First, the chamber was filled with water vapour. After a while, the air was added to achieve the desired total pressure. The difficulties in experiments with water vapour are well known. Adsorption and desorption processes lead to instability of the pressure, as well as humidity of the mixture. In our experiments, stability of the pressure was reached in approximately 10–12 hours after preparing the mixture. In spite of the reached stability of the mixture pressure, some uncontrolled processes might occur during preparation of the experiment and spectrum recording, which may lead to minor changes in the spectrometer baseline, for example, due to changes in temperature in the lab. These changes manifest themselves as smooth variations of the experimental spectrum. Existence of such variations was revealed at the data processing stage.

The water vapour adsorption–desorption processes lead to the uncertainty of the water vapour partial pressure $P_{\text{H}_2\text{O}}$ in the mixture. This value can be refined using a water vapour spectral line with well-known intensity. In our case, the high-frequency wing of the 183 GHz rotational water line (Fig. 1) can be used. (The line peak recording was impossible due to the limited operating range of the radiation source.) After recording the absorption spectra of the mixture in the 188–258 GHz range (which takes about 2 hours) we repeated recording of the line wing to control the water vapour content. The change in the water pressure was taken into account like in the earlier work,²¹ where the integrated intensity of this line was measured. Overlapping of the 183 GHz line wing with the dimer peak centred near 196 GHz reduced the accuracy of the obtained water vapour line intensity and its partial pressure.

The method of accounting for the monomer absorption was described in Section 3. After the calculated contribution of the monomer is subtracted from the observed spectrum, the remaining part can be considered to consist of three terms. One is responsible for the collisional interaction of $\text{H}_2\text{O}-\text{H}_2\text{O}$ molecules and proportional to squared water pressure ($P_{\text{H}_2\text{O}}^2$). Two other terms are due to the interaction of H_2O with N_2 and O_2 molecules, and proportional to the product of the corresponding gas component partial pressure and $P_{\text{H}_2\text{O}}$:

$$\alpha_{\text{int}} = C_{\text{H}_2\text{O}-\text{H}_2\text{O}} P_{\text{H}_2\text{O}}^2 + C_{\text{H}_2\text{O}-\text{N}_2} P_{\text{H}_2\text{O}} P_{\text{N}_2} + C_{\text{H}_2\text{O}-\text{O}_2} P_{\text{H}_2\text{O}} P_{\text{O}_2} \quad (21)$$

The so-called “dry continuum” caused by collisional interactions between N_2 and O_2 molecules can be neglected under the conditions of our experiments.⁴⁹ The continuum components linearly dependent on $P_{\text{H}_2\text{O}}$ were earlier investigated in a number of studies.^{22,50,51} Assume that this part of the continuum is caused by the $\text{H}_2\text{O}-\text{N}_2$ dimers by analogy with the water dimer; then, the low pressure spectrum of the mixture may contain spectral features of this heterodimer and/or the $\text{H}_2\text{O}-\text{O}_2$ complex.^{52,53} Since information on these spectra in the studied frequency range is not available, we restricted ourselves to the subtraction from the experimental spectrum of the smooth function corresponding to the linear-with-humidity

component of the continuum which was calculated on the basis of the results of the earlier studies.^{22,50}

The remaining component of the spectrum should include dimer peaks (we assumed that the integrated intensity and the width of the peaks are unknown) and the “pedestal”. The latter may vary with frequency independent of water dimers, which is caused by uncontrollable experimental effects and/or spectra of other molecular complexes. The influence of the pedestal was minimal for the spectra recorded at low air pressure. For example, the mixture spectral recording at 71.6 Torr (water vapour partial pressure, as determined from the wing of the 183 GHz line was 10.5 Torr) and 297.3 K after subtraction of the linear-with-humidity component of the continuum can be well described by a convolution model (13), in which the dimer spectral recording in pure water vapour was used as a starting one. The use of this model permitted estimating the air-broadening coefficient of the dimer peaks. The obtained value of $6.6(24)$ MHz Torr⁻¹ was a starting point for further evaluation of this parameter.

Application of the convolution model (13) for the approximation of the spectra recorded at a higher air pressure did not give good results, since the pedestal contribution in these spectra was rather large. To resolve the problem we found the pedestal empirically. This is possible assuming that typical variations of the pedestal with the frequency are much “slower” than the characteristic variations related to the dimer peaks. We used the following procedure. The water dimer spectrum corresponding to the experimental conditions was calculated using the convolution method (the starting value of the air-broadening parameter mentioned was used) and was subtracted from the observed spectrum. The remaining part was approximated by the sixth degree polynomial. Such an approximation picks out only large-scale frequency variations of the absorption, leaving the fine-scale variations due to incomplete subtraction of the dimer spectrum. The resulting polynomial function was considered to be the “empirical pedestal” and was subtracted from the original spectrum. The remaining absorption was analyzed using the convolution model (13) and the “Lorentzian” model (11).

Four spectra recorded at partial water vapour pressure of about 10 Torr and the gas mixture total pressure of 72, 86, 251 and 552 Torr were processed by this method. These spectra are shown in Fig. 13 together with the fitted functions of the convolution model (13).

Analyses of three spectra (corresponding to 72, 86 and 251 Torr) using the method described above and models (11) and (13) permitted determining the averaged air-broadening coefficient $\gamma_{\text{air}} = 6.3(21)$ MHz Torr⁻¹ and the bound water dimer equilibrium constant in air $K_{\text{Db}}^{\text{air}} = 1.0(2) \cdot K_{\text{Db}}^{\text{w}}$, where K_{Db}^{w} is the value obtained from the spectra in pure water vapour. Thus, our experiments confirmed that the amount of the bound water dimers in air is the same as in pure water vapour at the same partial pressure of water.

No dimer signatures were revealed in the 552 Torr spectrum due to the large collisional broadening (the estimated width of the dimer peaks exceeds the spacing between them). The expected spectrum calculated using the model parameters obtained from lower pressure spectra is shown in Fig. 13 by the dashed curve.

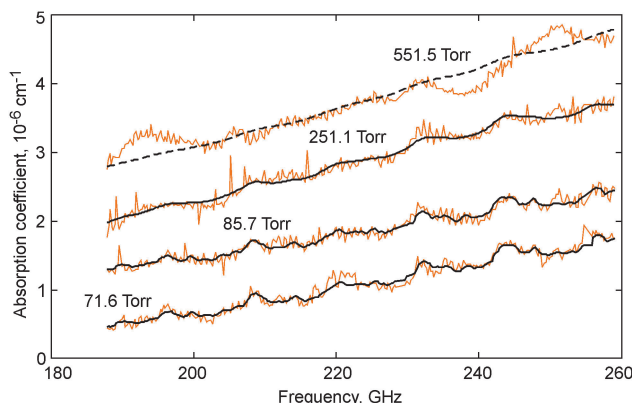


Fig. 13 Experimental spectra of the moist air continuum (thin orange curves) and the corresponding model functions calculated by the convolution method from the water dimer spectra recording in pure water vapour (thick black curves). Total mixture pressure values are shown near the corresponding spectrum. For figure clarity, the lower and upper traces are shifted down by 10^{-6} cm^{-1} and up by $5 \times 10^{-7} \text{ cm}^{-1}$, respectively.

The spectral inhomogeneities observed in this spectrum are most likely caused by the instrumental effects associated with the known difficulties in experiments with water vapour. Additional experiments are required for determining the nature of these peculiarities.

6. Conclusion

The use of the highly sensitive broadband resonator spectrometer facilitated obtaining unique experimental data which characterize the spectral properties of water dimers under close to atmospheric conditions. The sequence of six peaks was observed in the spectra of pure water vapour and in mixtures with air in the frequency range 188–258 GHz. The peaks represent a superposition of individual lines corresponding to rotational transitions of the bound water dimer. The observed sequence continues the series of four peaks observed in the previous work.¹⁴

The signal-to-noise ratio of the spectral recordings and reproducibility of the observed dimer features over a broad range of temperature (288–322 K) and water vapour pressure (3.7–34.2 Torr) constrain the shape of the “warm” water dimer spectrum in the studied range of frequencies. These spectra can be used as a reliable reference for improving the accuracy of *ab initio* calculations.

The numerical model based on the most accurate to date *ab initio* calculations of the bound dimer spectrum and the model based on convolution of the observed spectrum with the Lorentzian function were used for quantitative data analysis. The equilibrium constant of bound dimers, the dimer dissociation energy, and the self- and air-pressure broadening coefficients of dimer lines were determined. The contribution of the metastable states of the dimer to the observed absorption was assessed. Combined with the previously known data, results of the analysis allowed us to plot relative contributions of all possible pair states of water vapour molecules to the second

virial coefficient in the broad temperature range. All results are in good general agreement with the previous theoretical calculations and experimental data.

The result of this work, which is most important for spectroscopic applications, is the study of the dimer spectra in air. It has been experimentally confirmed that adding air to pure water vapour does not change the integrated intensity of the dimer spectrum but only decreases the contrast of the dimer peaks due to collisional broadening. This leads to important conclusions about the dimer abundance in the atmosphere and provides an opportunity to study their real role in atmospheric processes.

To conclude, it is worth noting that the shape of the water dimer spectrum defined in our laboratory experiments may serve as a starting point for searching for dimer signatures and studying their abundance in the real atmosphere using, for example, radiometric measurements as it was proposed by Odintsova *et al.*¹⁷

Acknowledgements

The authors are grateful to reviewers for many valuable comments and suggestions. We also thank A.A. Vigasin for many long and fruitful discussions on the subject of this paper. The work was partly supported by the Russian Foundation for Basic Research and by the Russian Academy of Sciences.

References

- 1 J. T. Kiehl and K. E. Trenberth, *Bull. Am. Meteorol. Soc.*, 1997, **78**, 197.
- 2 K. E. Trenberth, J. T. Fasullo and J. Kiehl, *Bull. Am. Meteorol. Soc.*, 2009, **90**, 311.
- 3 K. P. Shine, I. V. Ptashnik and G. Rädel, *Surv. Geophys.*, 2012, **33**, 535.
- 4 M. Herman and R. J. Saykally, *Mol. Phys.*, 2010, **108**, 2153.
- 5 I. V. Ptashnik, *J. Quant. Spectrosc. Radiat. Transfer*, 2008, **109**, 831.
- 6 I. V. Ptashnik, K. P. Shine and A. A. Vigasin, *J. Quant. Spectrosc. Radiat. Transfer*, 2011, **112**, 1286.
- 7 D. Mondelain, A. Aradj, S. Kassi and A. Campargue, *J. Quant. Spectrosc. Radiat. Transfer*, 2013, **130**, 381.
- 8 J. A. Odutola and T. R. Dyke, *J. Chem. Phys.*, 1980, **72**, 5062.
- 9 G. T. Fraser, R. D. Suenram and L. H. Coudert, *J. Chem. Phys.*, 1989, **90**, 6077.
- 10 E. Zwart, J. J. Ter Meulen and W. L. Meerts, *J. Mol. Spectrosc.*, 1991, **147**, 27.
- 11 F. N. Keutsch, L. B. Braly, M. G. Brown, H. A. Harker, P. B. Petersen, C. Leforestier and R. J. Saykally, *J. Chem. Phys.*, 2003, **119**, 8927.
- 12 N. Goldman, R. S. Fellers, C. Leforestier and R. J. Saykally, *J. Phys. Chem. A*, 2001, **105**, 515.
- 13 N. Goldman, C. Leforestier and R. J. Saykally, *J. Phys. Chem. A*, 2004, **108**, 787.
- 14 M. Yu. Tretyakov, E. A. Serov, M. A. Koshelev, V. V. Parshin and A. F. Krupnov, *Phys. Rev. Lett.*, 2013, **110**, 093001.

- 15 R. J. Saykally, *Physics*, 2013, **6**, 22.
- 16 Y. Scribano and C. Leforestier, *J. Chem. Phys.*, 2007, **126**, 234301.
- 17 T. A. Odintsova, M. Yu. Tretyakov, A. F. Krupnov and C. Leforestier, *J. Quant. Spectrosc. Radiat. Transfer*, 2014, **140**, 75.
- 18 M. Yu. Tretyakov, A. F. Krupnov, M. A. Koshelev, D. S. Makarov, E. A. Serov and V. V. Parshin, *Rev. Sci. Instrum.*, 2009, **80**, 093106.
- 19 V. V. Parshin, E. A. Serov, G. M. Bubnov, V. F. Vdovin, M. A. Koshelev and M. Yu. Tretyakov, *Radiophys. Quantum Electron.*, 2014, **56**, 554.
- 20 V. V. Parshin, M. Yu. Tretyakov, M. A. Koshelev and E. A. Serov, *Radiophys. Quantum Electron.*, 2009, **52**, 583.
- 21 M. Yu. Tretyakov, V. V. Parshin, M. A. Koshelev, V. N. Shanin, S. E. Myasnikova and A. F. Krupnov, *J. Mol. Spectrosc.*, 2003, **218**, 239.
- 22 M. A. Koshelev, E. A. Serov, V. V. Parshin and M. Yu. Tretyakov, *J. Quant. Spectrosc. Radiat. Transfer*, 2011, **112**, 2704.
- 23 L. S. Rothman, I. E. Gordon, Y. Babikov, A. Barbe, D. C. Benner and P. F. Bernath, *et al.*, *J. Quant. Spectrosc. Radiat. Transfer*, 2013, **130**, 4.
- 24 G. Yu. Golubiatnikov, *J. Mol. Spectrosc.*, 2005, **230**, 196.
- 25 F. C. De Lucia, P. Helminger, R. L. Cook and W. Gordy, *Phys. Rev. A: At., Mol., Opt. Phys.*, 1972, **5**, 487.
- 26 F. C. De Lucia, R. L. Cook, P. Helminger and W. Gordy, *J. Chem. Phys.*, 1971, **55**, 5334.
- 27 F. C. De Lucia, P. Helminger, R. L. Cook and W. Gordy, *Phys. Rev. A: At., Mol., Opt. Phys.*, 1972, **6**, 1324.
- 28 F. C. De Lucia and P. Helminger, *J. Mol. Spectrosc.*, 1975, **56**, 138.
- 29 G. Yu. Golubiatnikov, M. A. Koshelev and A. F. Krupnov, *J. Quant. Spectrosc. Radiat. Transfer*, 2008, **109**, 1828.
- 30 M. A. Koshelev, *J. Quant. Spectrosc. Radiat. Transfer*, 2011, **112**, 550.
- 31 M. Yu. Tretyakov, M. A. Koshelev, I. N. Vilkov, V. V. Parshin and E. A. Serov, *J. Quant. Spectrosc. Radiat. Transfer*, 2013, **114**, 109.
- 32 S. A. Clough, F. X. Kneizys and R. W. Davies, *Atmos. Res.*, 1989, **23**, 229.
- 33 Y. Scribano, N. Goldman, R. J. Saykally and C. Leforestier, *J. Phys. Chem. A*, 2006, **110**, 5411.
- 34 A. F. Krupnov, M. Yu. Tretyakov and C. Leforestier, *J. Quant. Spectrosc. Radiat. Transfer*, 2009, **110**, 427.
- 35 D. E. Stogryn and J. O. Hirschfelder, *J. Chem. Phys.*, 1959, **31**, 1531.
- 36 J. M. Calo and J. H. Brown, *J. Chem. Phys.*, 1974, **61**, 3931.
- 37 A. A. Vigasin, *Infrared Phys.*, 1991, **32**, 461.
- 38 Q. Ma, R. H. Tipping and C. Leforestier, *J. Chem. Phys.*, 2008, **128**, 124313.
- 39 C. Leforestier, R. H. Tipping and Q. Ma, *J. Chem. Phys.*, 2010, **132**, 164302.
- 40 H. M. Pickett, *Appl. Opt.*, 1980, **19**, 2745.
- 41 C. Leforestier, K. Szalewicz and A. van der Avoird, *J. Chem. Phys.*, 2012, **137**, 014305.
- 42 B. E. Rocher-Casterline, L. C. Ch'ng, A. K. Mollner and H. Reisler, *J. Chem. Phys.*, 2011, **134**, 211101.
- 43 L. A. Curtiss and D. J. Frurip, *J. Chem. Phys.*, 1979, **71**, 2703.
- 44 M. Yu. Tretyakov, E. A. Serov and T. A. Odintsova, *Radiophys. Quantum Electron.*, 2012, **54**, 700.
- 45 W. Wagner and A. Prüß, *J. Phys. Chem. Ref. Data*, 2002, **31**, 387.
- 46 C. Leforestier, *J. Chem. Phys.*, 2014, **140**, 074106.
- 47 A. A. Vigasin, *Weakly interacting molecular pairs: unconventional absorbers of radiation in the atmosphere*, ed. C. Camy-Peyret and A. A. Vigasin, Kluwer Academic Publishers, Netherlands, 2003, pp. 23–47.
- 48 A. A. Vigasin, *Mol. Phys.*, 2010, **108**, 2309.
- 49 J. Boissoles, C. Boulet, R. H. Tipping, A. Brown and Q. Ma, *J. Quant. Spectrosc. Radiat. Transfer*, 2003, **82**, 505.
- 50 H. J. Liebe and D. H. Layton, *Millimeter-Wave Properties of the Atmosphere: Laboratory Studies and Propagation modeling*, NTIA Report No. 87-224, 1987.
- 51 T. Kuhn, A. Bauer, M. Godon, S. Buhler and K. Kunzi, *J. Quant. Spectrosc. Radiat. Transfer*, 2002, **74**, 545.
- 52 A. A. Vigasin, *J. Quant. Spectrosc. Radiat. Transfer*, 2000, **64**, 25.
- 53 Yu. I. Baranov, I. A. Buryak, S. E. Lokshtanov, V. A. Lukyanchenko and A. A. Vigasin, *Philos. Trans. R. Soc., A*, 2012, **370**, 2691.